Induction motor modelling for load-frequency control system

AKBAR KARIMIPOUYA[1], **SHAHRAM KARIMI**[1,*], **AND HAMDI ABDI**[1]

[1] *Department of Electrical Engineering, Razi University, Kermanshah, Iran*
[*] *Corresponding author: shahramkarimi@razi.ac.ir*

Manuscript received 15 December, 2020; revised 07 September, 2021; accepted 21 September, 2021. Paper no. JEMT-2012-1269.

The accuracy of the load-frequency control (LFC) system depends on the accuracy of models used for the components that affect the frequency response. In the conventional LFC system, the frequency-sensitive loads, including induction motors, are simply modeled by the load-damping coefficient. The purpose of this paper is to obtain the fifth-, third- and first-order induction motors models for applying in the LFC system. Also, in this paper, the performance and accuracy of these models on the frequency response in a small-scale stand-alone microgrid are compared. In addition, the effect of system and motor parameters on the frequency response characteristics are investigated. The simulation results point out that the commonly used constant load-damping coefficient model can't always appropriately reflect the impact of the induction motors on the frequency response.

keywords: *Load-frequency control system, induction motor, frequency response.*

http://dx.doi.org/10.22109/jemt.2021.262149.1269

1. INTRODUCTION

The type and characteristics of electrical loads are the most important factors affecting power system frequency response, especially in the low-inertia stand-alone microgrids. Although the importance of load modeling with abundant research results in dynamic systems is widely known, it is still a very challenging problem needed to be improved due to the continuous complexity of the load component of industrial development. The load model and modeling method continuously improved with the continuous deepening of research [1]. Since frequency variation affects the electrical power of the frequency-sensitive loads, proper modeling of such loads is crucial in the load frequency control (LFC) system. Among the frequency-sensitive loads, induction motors can be considered as the most used ones in the power systems. About 20 to 30 percent of the electrical loads are induction motors and consume more than half of the total energy provided by an electrical system [2]. Due to the low inertia of MGs compared to the grid, maintaining an active and reactive power balance between supply and consumption, especially in the presence of motor loads and frequent load changes, is a challenge [3]. Proper modeling of the induction motors could lead to a more accurate LFC system. In the large-scale power systems, the frequency-sensitive loads, including induction motors, are simply modeled by the load-damping coefficient [4, 5]. Also, this simple model has been widely used in the LFC system of the stand-alone microgrids [6–8]. Even in [9], the linear relationship between active power and frequency changes has been further described, but induction motor dynamics have not been considered and just the static aspect has been studied. The static models of the induction motor simplify model the induction motor behavior using a load-damping coefficient. In addition, the load-damping coefficient is usually assumed as a constant under different operating points. However, in this paper, it is shown that a constant load-damping coefficient cannot present an accurate model for all induction motors when a significant disturbance has occurred in the low-inertia microgrids.

Recently, a few papers are being published to model the dynamics of induction motors in the LFC systems. In [10], the first-order induction motor model has been introduced, and is shown that the induction motor behaves similarly to the derivative-proportional when an active power disturbance is occurred. In [11], the same simplified first-order model has been examined in more detail, showing the coefficients that increase the sensitivity of the electromagnetic torque and affect the frequency response.

Dynamical model of a induction motor helps in understanding the physical behavior of the motor system [12]. Generally, all proposed methods for load modeling are categorized into frequency and time-domain methods. Most identification methods apply time-domain modeling to model the loads in the power systems [13, 14]. Load modeling involves two main steps: 1) selection of load model structure and 2) specifying the load model parameters using measurement-based methods [15]. a method for motor model order reduction is developed using

the Cauer ladder network (CLN) [16], but a commonly accepted model of an induction motor applicable to transient studies after a considerable event is the fifth-order Park model, which is also referred to as the two-axis model. For dynamic studies, it is more useful to apply low-order models, which decreases the complexity of the system. The order of the induction motor model can be reduced from 5 to 3 by ignoring the transient stator flux changes. This is called the neglecting stator transients model (NST). In the first-order model, the only variable is the rotor speed, and the electromechanical torque is a function of the rotor speed. To obtain the first-order model, the flux transient changes in both the stator and the rotor are ignored [17].

The purpose of this paper is to obtain the fifth-, third- and first-order induction motors models for applying in the LFC system. Also, in this paper, the performance and accuracy of these models on the frequency response in a small-scale stand-alone microgrid are investigated. Finally, this paper seeks to answer this question: is the commonly used constant load-damping coefficient model could appropriately reflect the impact of the induction motors on the frequency response in the small-scale stand-alone microgrids?

Point of views of this article are abbreviated as follows:

1- The eigenvalues of several small and large induction motors are obtained for the first-, third- and fifth-order models and by using the bode diagram and eigenvalues it is concluded that always cannot use the first-order model instead of the fifth-order model. But by applying several conditions, this model can be replaced. In [10, 11], these subjects have not been followed and have directly used the first-order induction motor model.

2- The reduced model is applied to the LFC system after conversion to a simpler form, and the effects of the induction motor on the frequency response are analyzed. The remainder of this paper is organized as follows: The first-, third-, and fifth-order models of induction motors for applying in the LFC system are presented in Section 2. In Section 3 these models are compared through their Bode diagrams. The performance and accuracy of these three models and the conventional model on the frequency response in a stand-alone microgrid are surveyed in Section 4. Finally, the conclusion is presented in Section 5.

2. INDUCTION MOTOR MODELING

A. Park Model (5th Model)

The standard park model requires some simple assumptions, as following: - The device is designed to have a smooth air gap. - The considered winding has a sinusoidal distribution over the surface of the air gap. - The saturation and skin effects are ignored.

By applying these assumptions, the equations of the Park model for an induction machine are as follows:

$$u_s = i_s R_s + \frac{d\varphi_s}{dt} + j\omega_k \varphi_s \tag{1}$$

$$0 = i_r R_r + \frac{d\varphi_r}{dt} + j(\omega_k - p\omega_m)\varphi_r \tag{2}$$

$$J_m \frac{d\omega_m}{dt} = T_e - T_s \tag{3}$$

$$T_e = p\mathrm{Im}(\varphi_s * i_s) \tag{4}$$

Where i_s and i_r are the stator and rotor current vectors, respectively, ω_m is the rotor mechanical speed and ω_k is the angular speed of the coordinate system. T_s is the torque applied to the shaft, T_e is the electromechanical torque, and u_s is the source voltage vector. R_s and R_r are the rotor and stator resistances, respectively. J_m is the moment of inertia of the motor and p is the number of pairs of poles. Rotor and stator leakage flux vectors are as follows:

$$\varphi_s = L_s i_s + L_m i_r = (L_{s\lambda} + L_m) i_s + L_m i_r \tag{5}$$

$$\varphi_r = L_r i_r + L_m i_s = (L_{r\lambda} + L_m) i_r + L_m i_s \tag{6}$$

L_s, L_r, and L_m are the inductances of the stator, rotor and magnetic, respectively. $L_{s\lambda}$ and $L_{r\lambda}$ are the leakage inductances of the stator and rotor. Leakage flux equations can be used instead of the current equations as the state variables, by replacing (5) and (6) in (1) and (2), one can deduce

$$u_s = \left[\frac{R_s}{L_s'} + j\omega_s\right]\varphi_s + \frac{d\varphi_s}{dt} - k_r \frac{R_s}{L_s'}\varphi_r \tag{7}$$

$$0 = -k_s \frac{R_r}{L_r'}\varphi_s + \left[\frac{R_r}{L_r'} + j(\omega_s - p\omega_m)\right]\varphi_r + \frac{d\varphi_r}{dt} \tag{8}$$

The electromechanical torque can be expressed as follows.

$$T_e = p\frac{k_r}{L_s'}\mathrm{Im}(\varphi_s \varphi_r^*) \tag{9}$$

In addition, the motion equation is:

$$J_m \frac{d\omega_m}{dt} = T_e - T_s \tag{10}$$

Equations (7) and (8) can be represented in dq frame. Since the voltage changes are ignored in the LFC systems ($\Delta u_{sd}, \Delta u_{sq} \cong 0$), we can obtain the fifth-order Park model around the induction motor operating point. In this model, the stator and rotor flux changes and the rotor speed changes are the state variables and the frequency and the motor torque changes are the input variables.

$$\begin{aligned} \dot{X} &= AX + BU \\ Y &= CX + DU \end{aligned} \tag{11}$$

Where

$$X = \begin{bmatrix} \Delta\varphi_{sd} \\ \Delta\varphi_{sq} \\ \Delta\varphi_{rd} \\ \Delta\varphi_{rq} \\ \Delta\omega_m \end{bmatrix}, \quad U = \begin{bmatrix} \Delta\omega_s \\ \Delta T_s \end{bmatrix} \tag{12}$$

$$A = \begin{bmatrix} -\frac{R_s}{L_s'} & \omega_{S0} & \frac{K_r R_s}{L_s'} & 0 & 0 \\ -\omega_{S0} & -\frac{R_s}{L_s'} & 0 & \frac{K_r R_s}{L_s'} & 0 \\ \frac{K_s R_r}{L_r'} & 0 & -\frac{R_r}{L_r'} & \omega_{S0} - p.\omega_{m0} & -p.\varphi_{rq0} \\ 0 & \frac{K_s R_r}{L_r'} & -(\omega_{S0} - p.\omega_{m0}) & -\frac{R_r}{L_r'} & p.\varphi_{rd0} \\ -\frac{pK_r\varphi_{rq0}}{L_s' J_m} & \frac{pK_r\varphi_{rd0}}{L_s' J_m} & \frac{pK_r\varphi_{sq0}}{L_s' J_m} & -\frac{pK_r\varphi_{sd0}}{L_s' J_m} & 0 \end{bmatrix} \tag{13}$$

$$B = \begin{bmatrix} \varphi_{sq0} & 0 \\ -\varphi_{sd0} & 0 \\ \varphi_{rq0} & 0 \\ -\varphi_{rd0} & 0 \\ 0 & -\frac{1}{J_m} \end{bmatrix} \quad (14)$$

$$C = \begin{bmatrix} -\frac{pK_r\varphi_{rq0}}{L_s'} & \frac{pK_r\varphi_{rd0}}{L_s'} & \frac{pK_r\varphi_{sq0}}{L_s'} & -\frac{pK_r\varphi_{sd0}}{L_s'} & 0 \end{bmatrix} \quad (15)$$

$$D = 0 \quad (16)$$

B. Third-order model

Ignoring the transient stator flux changes ($d\varphi_{sd}/dt = 0$, $d\varphi_{sq}/dt = 0$), the order of the induction machine can be reduced from 5 to 3. Considering this assumption, the state and input variables, and other parameters in the state space equation (11) for the 3^{rd} order model of induction machine will be obtained as the following:

$$X = \begin{bmatrix} \Delta\varphi_{rd} \\ \Delta\varphi_{rq} \\ \Delta\omega_m \end{bmatrix}, \; U = \begin{bmatrix} \Delta\omega_s \\ \Delta T_s \end{bmatrix}, \; \Delta u_{sd}, \Delta u_{sq} \cong 0 \quad (17)$$

$$A = \begin{bmatrix} A1 & B1 & C1 \\ A2 & B2 & C2 \\ \frac{A3}{J_m} & \frac{B3}{J_m} & \frac{C3}{J_m} \end{bmatrix}, \; B = \begin{bmatrix} D1 & 0 \\ D2 & 0 \\ \frac{D3}{J_m} & -\frac{1}{J_m} \end{bmatrix} \quad (18)$$

$$C = \begin{bmatrix} A3 & B3 & C3 \end{bmatrix}, \; D = \begin{bmatrix} D3 & 0 \end{bmatrix} \quad (19)$$

The parameters *A1*, *A2*, *A3*, *B1*, *B2*, *B3*, *C1*, *C2*, *C3*, *D1*, *D2*, and *D3* are presented in appendix.

C. The first-order model

In the first-order model, the state variable is the rotor speed, and the flux transient changes in both the stator and the rotor are ignored. The state equations in this model are obtained as follows:

$$\Delta T_e = (A3 * S1 + B3 * S3)\,\Delta\omega_m + (A3 * S2 + B3 * S4 + D3)\,\Delta\omega_s \quad (20)$$

$$\dot{\Delta\omega_m} = \frac{(A3*S1+B3*S3)}{J_m}\Delta\omega_m + \frac{(A3*S2+B3*S4+D3)}{J_m}\Delta\omega_s - \frac{\Delta T_s}{J_m} \quad (21)$$

The parameters *S1*, *S2*, *S3*, and *S4* are presented in appendix.

3. COMPARATIVE STUDY

s mention in Section 2, the mechanical torque and the grid frequency changes are considered as the input variables. The electrical torque of the induction motor will have changed, if any of these input variables change. Another variable that can affect the motor's power is the motor voltage. Since the frequency changes do not have a significant effect on the voltage, the voltage changes are disregarded in the LFC systems.

Disregarding the voltage changes, to compare these models, in this paper, two transfer functions include $\Delta T_e/\Delta T_s$ and $\Delta T_e/\Delta\omega_s$ are obtained for every three models. In addition, this investigation is performed for the low- and high-power induction motors. The specifications of the considered induction motors are presented in Table 1 [18]. Fig. 1 shows the bode diagrams for the high-power induction motor) 250hp motor (. As can be seen, the first-order model is identical to the fifth-order model up to about 5 Hz. The third-order model has also the behavior similar to the 5th order around 12 Hz.

For the low-power motor (3hp motor), the bode diagrams are plotted in Fig. 2. As one can see, in this case, the first-order model behaves similar to the fifth-order model up to a frequency about 10 Hz. In addition, the first-order model has the same behavior as the third-order model up to 30 Hz.

The eigenvalues of the investigated induction motors for the three models of 11 induction motors in the nominal operating point are given in Table 2. Two pairs of complex conjugate eigenvalues of the fifth-order model, are related to the transient stator and rotor flux changes, and the negative real eigenvalue is the eigenvalue corresponding to the rotor speed. In the 3^{rd}-order model, the complex conjugate eigenvalues corresponding to the transient stator flux changes are ignored. And in the first-order model, only the eigenvalue related to the rotor speed remains. Table 2 shows that first-order models for motors over 100hp are not very accurate. This is mainly due to the relatively smaller separation between the eigenvalues in the second column. This means that the traditional quasi-steady-state circuit representation of the algebraic equations corresponding to (1,2) may not be valid for larger machines. Since these algebraic equations are only the zeroth-order approximation of the corresponding integral manifolds, there is a need to go to higher-order corrections in order to improve the accuracy of the first-order models [19]. The eigenvalues obtained in table 2 are almost similar to the values in [19, 20], and it can be concluded that these values are reasonable.

To examine the dynamics of an induction motor, the LFC system shown in Fig. 3 is considered, which includes a synchronous generator with constant time T_g and T_t, which are related to the governor and turbine. The inertia of the synchronous generator is indicated by the inertia H. And R is the drop of the synchronous generator governor. The studied system parameters are presented in Table 3.

As can be seen in Fig. 3, there are two types of loads for this system. The first type is the static loads that are sensitive to

frequency changes and are shown with a sensitivity factor D, and the second type is a dynamic load, which is an induction motor. The induction motor is represented with two transfer functions, $\Delta T_e/\Delta\omega_s$ represents the electrical torque changes with respect to the frequency changes, and $\Delta T_e/\Delta T_s$ indicates the electrical torque changes with respect to the motor torque changes. These two transfer functions are obtained in Section 2 for the first, third, and fifth-order models.

The impact of these three models on the LFC frequency response

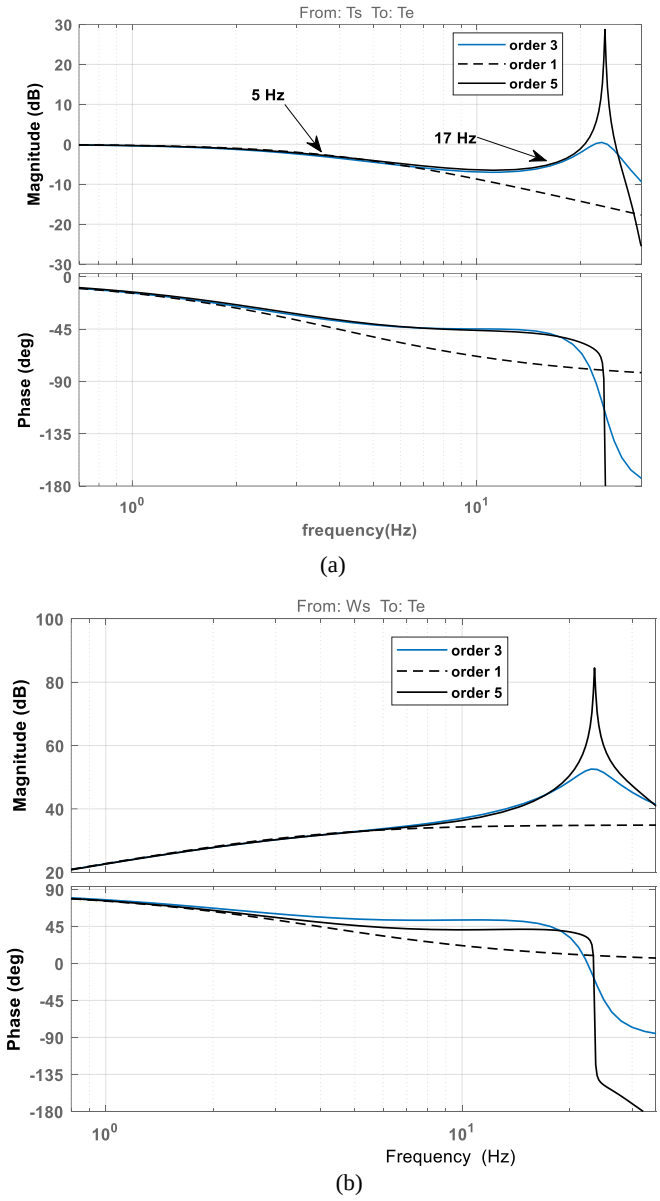

Fig. 1. Bode diagrams for the induction motor 250hp:
(a) $\Delta T_e/\Delta T_s$, (b) $\Delta T_e/\Delta\omega_s$

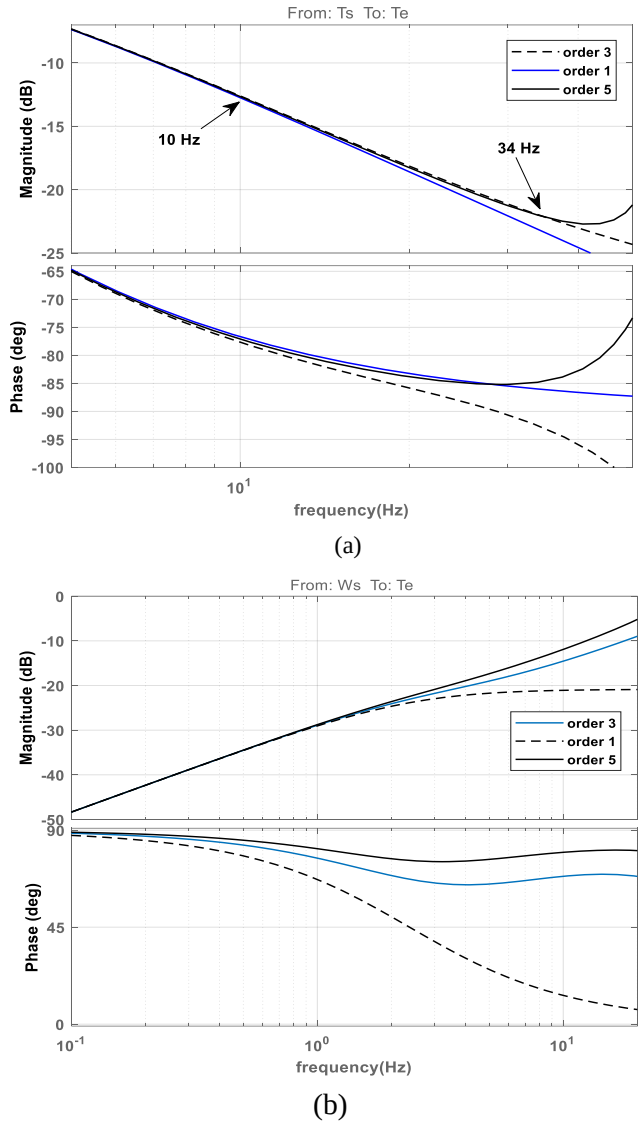

Fig. 2. Bode diagrams for the induction motor 3hp:
(a) $\Delta T_e/\Delta T_s$, (b) $\Delta T_e/\Delta\omega_s$

respect to 0.2 pu step change in the motor torque are shown in figures 4 and 5 for two motors with J_m = 0.089 and J_m = 6.91. Fig. 4 depicts that the system frequency response for the first-, third-, and fifth-order models of the motor with J_m = 0.089 are quite similar. But as shown in Fig. 5, when the moment of inertia of the motor is 6.91 (high-power motor), due to the zero-order estimation of the manifold, the first-order model results in a different frequency response than the third- and fifth-order models.

4. SIMPLIFIED INDUCTION MOTOR MODELING IN LFC SYSTEM

Considering (20) and (21), the terms H1, H2, H3, and H4 are defined as follows:

$$H_1 = (A3 * S1 + B3 * S3) \tag{22}$$

$$H_2 = (A3 * S2 + B3 * S4 + D3) \tag{23}$$

$$H_3 = (A3 * S1 + B3 * S3) \tag{24}$$

$$H_4 = (A3 * S2 + B3 * S4 + D3) \tag{25}$$

Using defined terms, (20) and (21) can represented as follows:

$$\Delta T_e = H_1\Delta\omega_m + H_2\Delta\omega_s \tag{26}$$

$$sJ_m\Delta\omega_m = H_3\Delta\omega_m + H_4\Delta\omega_s - \Delta T_s \tag{27}$$

Considering the input equal to zero, one can deduce:

$$\Delta\omega_m = \frac{H_4}{J_m s - H_3}\Delta\omega_s \tag{28}$$

Table 1. Specifications of the investigated induction motors [18]

Motor	*hp*	*P*	$V_{LL}(volt)$	$R_s(\Omega)$	$R_r(\Omega)$	$\chi_{ls}(\Omega)$	$\chi_{lr}(\Omega)$	$\chi_m(\Omega)$	$J_m(kgm^2)$	$H_m(s)$
1	3	4	220	0.434	0.815	0.754	0.754	26.12	0.089	0.7065
2	25	4	460	0.248	0.535	0.565	0.565	22.13	0.55	0.5277
3	50	4	460	0.086	0.228	0.301	0.301	11.51	1.66	0.7916
4	100	4	460	0.0309	0.133	0.150	0.150	7.12	4.44	1.0595
5	250	4	2300	0.68	0.399	2.45	2.45	8.58	6.91	0.6590
6	500	4	2300	0.262	0.187	1.206	1.206	52.02	11.06	0.5269
7	800	4	2300	0.131	0.0939	0.716	0.716	36.07	21.26	0.6329
8	1000	4	2300	0.112	0.073	0.603	0.603	54.13	29.86	0.7113
9	1500	4	2300	0.055	0.036	0.376	0.376	19.86	44.50	0.7072
10	2250	4	2300	0.0289	0.022	0.226	0.226	13.04	63.86	0.6760
11	6000	4	4160	0.022	0.022	0.301	0.301	22.20	674.94	2.6790

*hp: horsepower *P: poles/phase *VLL: line-to-line voltage

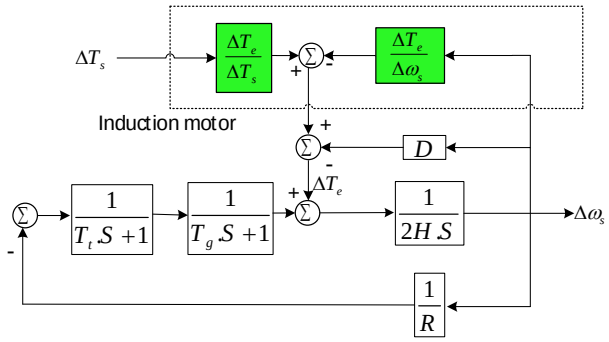

Fig. 3. LFC system with induction motor dynamics.

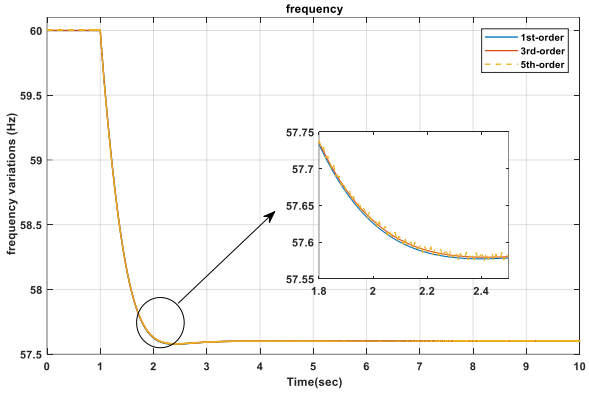

Fig. 4. LFC frequency response in the presence of a motor with J_m=0.089

$$\Delta T_e = H_1.\frac{H_4}{J_m s - H_3}\Delta\omega_s + H_2.\Delta\omega_s \tag{29}$$

The relationship between frequency and torque changes can be obtained as equation (30):

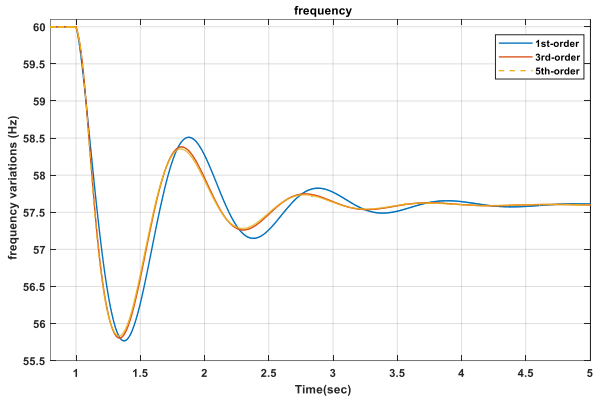

Fig. 5. LFC frequency response in the presence of a motor with J_m=6.91

$$\frac{\Delta T_e}{\Delta\omega_s} = H_2 + \frac{H_1.H_4}{J_m s - H_3} = H_2 + (-\frac{H_1.H_4}{H_3}).\frac{1}{(-\frac{J_m}{H_3})s+1} \tag{30}$$

If (30) reconstructed to the standard form, it becomes as shown in (31). Which $K_{e1} = H_2$, $K_{e2} = H_1.H_4/(-H_3)$, and $T_m = J_m/(-H_3)$. In addition, $K_0 = K_{e1}$ is the initial value at $t = 0^+$, $K_\infty = K_{e1} + K_{e2}$ is the steady state value, and the time constant T_m is related to the motor inertia.

$$\frac{\Delta T_e}{\Delta\omega_s} = K_{e1} + \frac{K_{e2}}{T_m s + 1} = K_0 + \frac{K_\infty - K_0}{T_m s + 1} \tag{31}$$

To verify the accuracy of the simplified first-order model, a fifth-order non-linear 3-phase motor is considered that connected to an AC voltage source. The model of 3-phase induction motor and AC voltage source is simulated using Sim Power System toolbox in Simulink environment. The induction motor is selected from Table 1 and has J_m = 0.089. Here, since the voltage amplitude is constant, the effect of the voltage change is ignored. The constant values of the first-order model are $K_\infty = 0$, $K_0 = 9.51$ and $T_m = 0.052\,s$. Fig. 6 shows the electrical torque changes when the frequency of the voltage

Table 2. Induction motor eigenvalues for the three models

Motor	5^{th}-order	3^{th}-order	1^{th}-order
	- 18.90 ±335.73i	-	-
1	- 289 ±287.8i	- 183.03 ±299.2i	-
	- 17.03	- 16.91	- 19.02
	- 2.77 ±360.50i	-	-
2	- 327.94 ±397.85i	- 206.09 ±441.36i	-
	- 26.68	- 25.26	- 22.04
	- 2.64 ±376.79i	-	-
3	- 186.40 ±402.74i	- 131.81 ±421.91i	-
	- 20.28	- 20.01	- 22.04
	- 1.63 ±376.90i	-	-
4	- 198.37 ±396.03i	- 159.10 ±412.58i	-
	- 16.22	- 16.09	- 17.20
	- 59.21 ±373.55i	-	-
5	- 18.97 ±56.62i	- 18.93 ±56.30i	-
	- 30.42	- 30.20	- 68.06
	- 41.68 ±373.69i	-	-
6	- 15.71 ±68.33i	- 15.73 ±67.97i	-
	- 27.19	- 26.98	- 104.5
	- 35.00 ±374.64i	-	-
7	- 13.36 ±64.35i	- 13.38 ±64.11i	-
	- 22.87	- 22.74	- 99.41
	- 35.37 ±374.78i	-	-
8	- 12.41 ±59.71i	- 12.43 ±59.49i	-
	- 20.73	- 20.62	- 86.42
	- 27.94 ±375.63i	-	-
9	- 9.76 ±61.84i	- 9.805 ±61.70i	-
	- 16.69	- 16.63	- 97.96
	- 24.39 ±375.79i	-	-
10	- 31.07 ±41.11i	- 31.03 ±41.001i	-
	- 25.27	- 25.20	- 99.64
	- 13.87 ±376.53i	-	-
11	- 7.21 ±27.41i	- 7.19 ±27.381i	-
	- 13.32	- 13.31	- 15.28

Table 3. Studied system parameters

Value	Parameter	Value	Parameter
0.08	$T_g(s)$	1	$D(Pu/Hz)$
0.15	$T_t(s)$	2	$2H(Pus)$
25	$R(Hz/Pu)$		

source is changed 0.02 pu at $t = 1$ s. Fig. 6 depicts that for this motor the first-order model behaves almost like a simulated fifth-order model. But for the larger motors, these difference become more apparent and for the motors with the power more than 100hp, the difference is quite noticeable.

A. Effect of parameters on the frequency response

a *Frequency deviation in the steady-state*

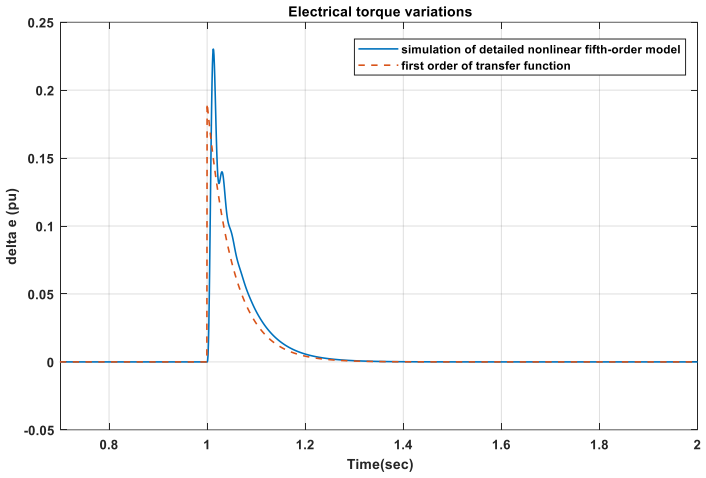

Fig. 6. Electric torque changes respect to the frequency step changes.

If a step disturbance $\Delta P_L(s) = \Delta P_L/s$ is applied to the system and all frequency-dependent loads including induction motors are modeled by the constant load-damping coefficient D, the frequency deviation is obtained using (32).

$$\Delta\omega(s) = \Delta P_L(s)\left[\frac{\frac{1}{2Hs+D}}{1+\left(\frac{1}{(2Hs+D)}\right)\left(\frac{1}{(T_ts+1)(T_gs+1)R}\right)}\right] \tag{32}$$

In the steady state, the frequency deviation can be deduce as follows.

$$\Delta\omega(t)|_{t=\infty} = \frac{\Delta P_L}{D+\frac{1}{R}} \tag{33}$$

If the first-order model is used to model the induction motor (as shown in Fig. 3), the system's frequency response is obtained as follows:

$$\Delta\omega(s) = \Delta P_L(s)\left[\frac{\frac{1}{2Hs+(K_0+\frac{K_\infty-K_0}{T_ms+1})+D}}{1+\left(\frac{1}{2Hs+(K_0+\frac{K_\infty-K_0}{T_ms+1})+D}\right)\left(\frac{1}{(T_ts+1)(T_gs+1)R}\right)}\right] \tag{34}$$

In this case, the frequency deviation in steady state can be calculated as follows.

$$\Delta\omega(\infty) = \lim_{S\to 0} s\frac{\Delta P_L}{s}\Delta\omega(s) = \frac{\Delta P_L}{K_\infty + D + \frac{1}{R}} \tag{35}$$

Equation (35) shows that when the induction motor is modeled as a dynamic frequency-dependent load, the frequency deviation in the steady state also depends on the factor K_∞. As can be seen from (34) the frequency deviation in the steady state does not depend on the inertia of the motor.

b *Maximum rate of change of frequency (ROCOF)*

For equations (32) and (34), ROCOF can be obtained using (26)

$$\left.\frac{d\Delta\omega}{dt}\right|_{t=0^+} = \lim_{s\to\infty} s\Delta\omega(s) - \Delta\omega(t)|_{0^-} = \frac{\Delta P_L}{2H} \qquad (36)$$

Equation (36) shows that ROCOF is inversely proportional to the system inertia H and the inertia of the induction motor has no effect on its value.

c *Effect of system parameters on the frequency response*

The effect of system parameters on the frequency response are depicted in Figs. 7 to 9. Fig. 7 illustrates that, with decreasing the system inertia from H = 1.5 s to H = 1 s, the accuracy of the first-order model is reduced. Fig. 8 depicts the results for the case where the 250 hp induction motor is modeled either using a first-order model or by a damping factor D. As can be seen in Fig. 8, if the induction motor is removed from the studied system, the steady-state frequency deviation and the frequency response is changed. The steady state frequency deviation can be estimated by a damping coefficient, which in this case the impact of the induction motor on the steady-state frequency deviation can be modeled by D = 1. Despite the accurate frequency deviation in the steady state when the induction motor is modeled by a D-factor, the frequency response is still different with the case that the induction motor is modeled by a first-order model. Fig. 8 shows that, the frequency nadir in the case that the induction motor is modeled by a first-order model is 56.7 Hz but if the induction motor is modeled by D = 1, the frequency nadir is equal to 57.9 Hz.
Fig. 9 presents that, with increasing the system inertia, the frequency response of first-order model and D-factor model become closer. Therefore, it can be concluded that the damping factor D can be used instead of the induction motors when the system inertia is large enough.
The parameters T_g, T_t and R can change over the time, or their actual values may differ from those intended at the design stage. Figures 10 to 12 show the uncertainty effects of these three parameters on the MG frequency response. Fig. 10 depicts the effect of a 50% change in R. As one can see in this figure, decreasing the value of R reduces the MG stability and increases the difference between obtained results from the first-order model with those obtained from 3^{rd}-order and 5^{rd}-order models. Also, increasing the value of R leads to more frequency deviation, but it brings the first-order model accuracy closer to the higher-order models. Fig. 11 and 12 illustrate the MG frequency response considering T_g and T_t variations, respectively. As one can see, the augmentation of the governor and turbine time constant degrade the MG dynamic response. And the effect of changing the turbine time constant is similar to the governor time constant.

d *Effect of motor parameters on the frequency response*

Motor inertia is directly related to J_m and is calculated from the relation $H_m = J_m\omega_0^2/2S_b$. Fig. 13 shows that in the same initial conditions, by increasing the inertia of the motor, the frequency undershoot is reduced. However, motor inertia does not affect the steady state frequency deviation, and ROCOF for all cases are the same value. As one can see in Table 4, with increasing inertia of the induction motor, the frequency of the oscillations decreases, and the damping coefficient increases, which is more evident in the pole of

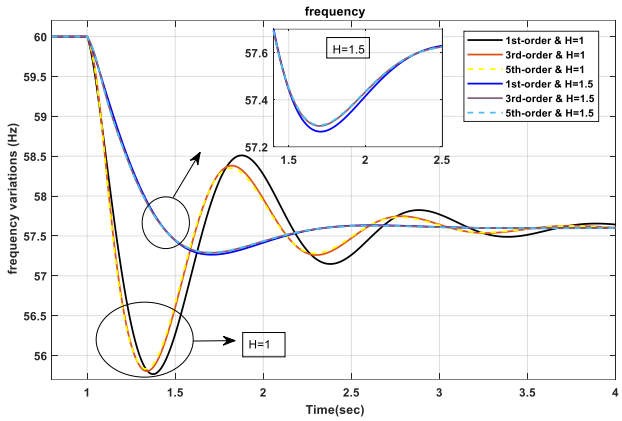

Fig. 7. Frequency response by changing the system inertia in the presence of a 250hp motor.

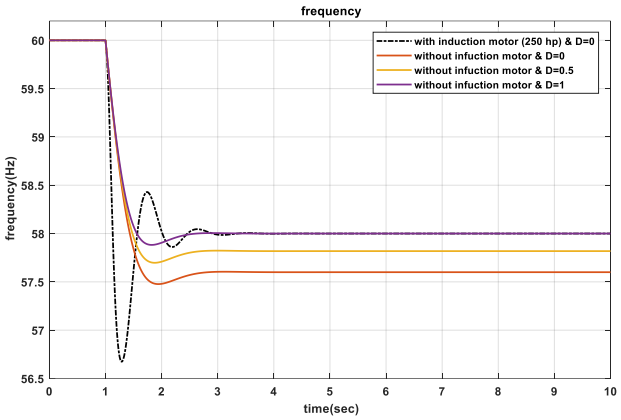

Fig. 8. Frequency response by changing the parameter D in the presence and without the motor 250hp and H = 1s.

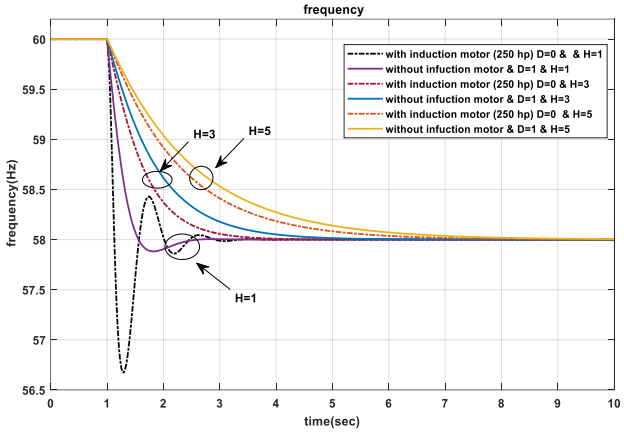

Fig. 9. Frequency response by changing the H parameter in the presence and without the motor 250hp.

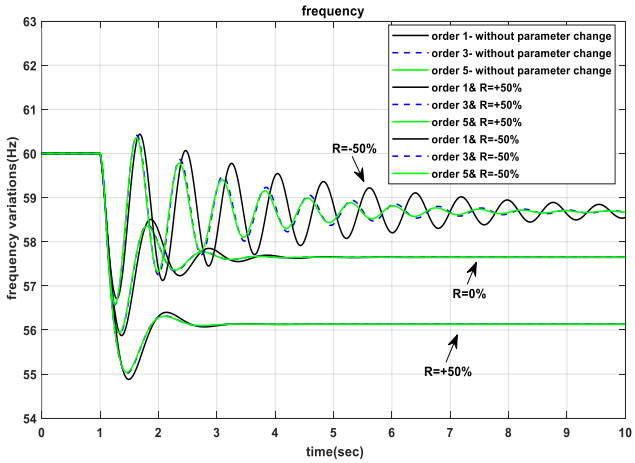

Fig. 10. MG frequency response considering R variations

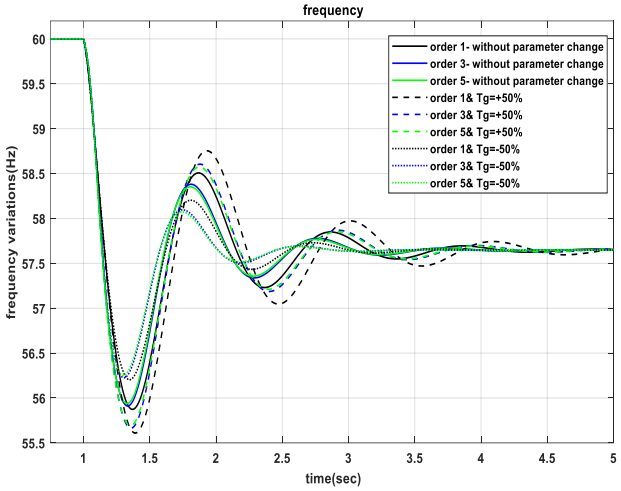

Fig. 11. MG frequency response considering T_g variations

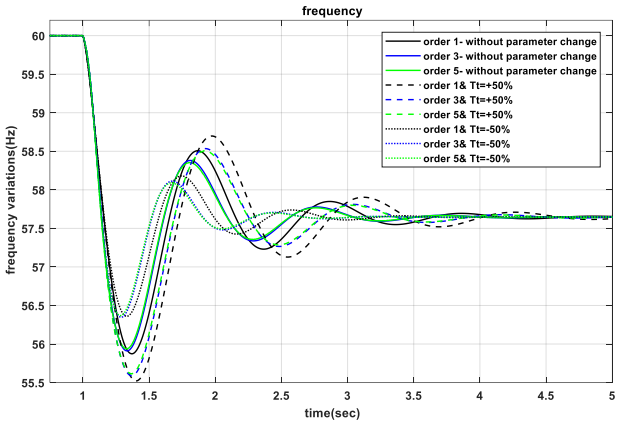

Fig. 12. MG frequency response considering T_t variations

the first-order model.

Fig. 14 illustrates the influence of K_∞, and K_0 coefficients of the first-order model on the frequency response. According to this figure, decreasing K_∞ increases the steady state frequency deviation, but does not significantly affect the ROCOF. Contrary, by changing the value of K_0, the steady-state frequency deviation does not change, but it will have a small effect on the frequency damping.

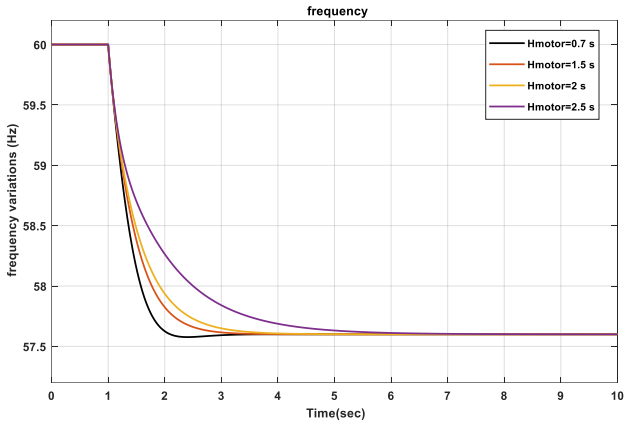

Fig. 13. Influence of induction motor inertia on frequency response.

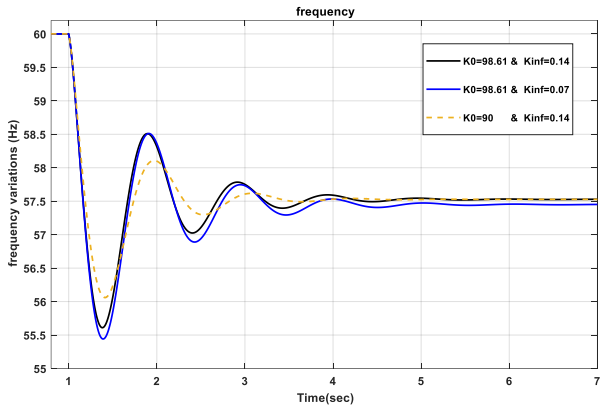

Fig. 14. Influence of K_∞ and K_0 parameters of the first-order model on the frequency response.

5. CONCLUSION

This paper uses the park model to provide a reduced model for the induction motor. By adding this model to the LFC system, the effect of parameters such as network inertia, motor inertia and coefficients of motor transfer function on the system frequency were examined. Using the bode-diagram and the eigenvalues of the induction motor, it was found that first-order model for high-power motors (above 100 hp) is not very accurate, but if the system inertia is high enough, the first-order model will behave closely to third- and fifth-models. In addition, this paper shows that although the steady-state frequency deviation is the same for both modeling with the constant damping coefficient and the first-order model, the frequency nadir will be different when the system inertia is low.

REFERENCES

1. X. Tian, X. Lii, L. Zhao, Z. Tan, S. Luo and C. Li, "Simplified Identification Strategy of Load Model Based on Global Sensitivity Analysis," IEEE Access, vol. 8, pp. 131545-131552, 2020.

Table 4. Studied system parameters

$H_m(s)$	Eigenvalue	Damping ratio	Frequency (rad/s)
	$-289 \pm 287.8i$	0.71	408
0.7	$-18.90 \pm 335.73i$	0.0562	336
	-17.03	1	17
	$-292 \pm 278i$	0.724	403
1.5	$-21 \pm 330i$	0.0634	331
	-8.5	1	8.5
	$-292 \pm 275i$	0.728	402
2	$-21.5 \pm 329i$	0.0652	330
	-6.46	1	6.46
	$-293 \pm 274i$	0.73	401
2.5	$-21.9 \pm 328i$	0.0664	329
	-5.21	1	5.21

2. Kundur P. Power System Stability and Control. New York: McGraw-Hill; 1994.
3. M. Khooban, T. Niknam, M. Shasadeghi, T. Dragicevic and F. Blaabjerg, "Load Frequency Control in Microgrids Based on a Stochastic Noninteger Controller," IEEE Transactions on Sustainable Energy, vol. 9, no. 2, pp. 853-861, 2018.
4. H. Huang, F. Li, "Sensitivity analysis of load damping characteristic in power system frequency regulation," IEEE Transactions on Power Systems, vol. 28. no. 2, pp. 1324-1335, 2013.
5. C. Pardhan, C. N. Bhende, "Frequency sensitivity analysis of load damping coefficient in wind farm-integrated power system," IEEE Transactions on Power Systems, vol. 32. no. 2, pp. 1016-1029, 2017.
6. M. Č. Bošković, T. B. Šekara, M. R. Rapaić, "Novel tuning rules for PIDC and PID load frequency controllers considering robustness and sensitivity to measurement noise," International journal of Electrical Power and Energy Systems, vol. 114, 2020.
7. A. Karimipouya, S. Karimi, H. Abdi, "Microgrid frequency control using the virtual inertia and ANFIS-based Controller", International Journal of Industrial Electronics, Control and Optimization, vol. 2, no. 2, pp. 145-154, 2019.
8. H. Bevrani, M. R. Feizi, and S. Ataee, "Robust frequency control in an islanded micro-grid: H/u synthesis approaches," IEEE Transactions on Smart Grid, vol. 7, no. 2, pp. 706-717, 2016.
9. A. R. Khatib, M. Appannagari, S. Manson and S. Goodall, "Load modeling assumptions: what is accurate enough?," IEEE Transactions on Industry Applications, vol. 52, no. 4, pp. 3611-3619, 2016.
10. Sigrist L, Rouco L. , "An induction motor model for system frequency response models," International transactions on Electrical Energy Systems, vol. 27, no. 11, e2413, 2017.
11. L.Chen, X. Wang, Y. Min, G. Li, L. Wang, J. Qi, F. Xu, "Modelling and investigating the impact of asynchronous inertia of induction motor on power system frequency response", International Journal of Electrical Power & Energy Systems, vol. 117, 2020.
12. R. S. C. Pal and A. R. Mohanty, "A Simplified Dynamical Model of Mixed Eccentricity Fault in a Three-Phase Induction Motor," IEEE Transactions on Industrial Electronics, vol. 68, no. 5, pp. 4341-4350, 2021.
13. X. Liang, C. Y. Chung, "Bus-split algorithm for aggregation of induction motors and synchronous motors in dynamic load modeling", IEEE Transactions on Industry Applications, vol. 50, no. 3, pp. 2115- 2126, 2014.
14. D. Ruiz-Vega; T.I. Asiain Olivares ;D. Olguin Salinas. "An approach to the initialization of dynamic induction motor models", IEEE Transactions on Power Systems, vol. 17, no. 3, pp. 747-751, 2002.
15. A. Gaikwad, P. Markham and P. Pourbeik, "Implementation of the WECC Composite Load Model for utilities using the component-based modeling approach," in Proc IEEE/PES Transmission and Distribution Conf. and Expo., Dallas, TX, pp. 1-5, 2016.
16. T. Matsuo, K. Sugahara, A. Kameari and Y. Shindo, "Model Order Reduction of an Induction Motor Using a Cauer Ladder Network," IEEE Transactions on Magnetics, vol. 56, no. 3, pp. 1-4, 2020.
17. P. C. Krause et all, "Analysis of electric machinery and drive systems", Wiley online library, 2002.
18. N. K. Roy, H. R. Pota, M. A. Mahmud, M. J. Hossain, "Key factors affecting voltage oscillations of distribution networks with distributed generation and induction motor loads", International Journal of Electrical Power & Energy Systems, vol. 53, pp. 515-528, 2013.
19. E. Drennan, S. Ahmed-Zaid and P. W. Sauer, "Invariant manifolds and start-up dynamics of induction machines," The Proceedings of the Twenty-First Annual North American Power Symposium, pp. 129-138 Rolla, MO, USA, 1989.
20. S. Ahmed-Zaid ; M. Taleb , "Structural modeling of small and large induction machines using integral manifolds", IEEE Transactions on Energy Conversion, vol. 6, no. 3, pp. 529-535, 1991.

APPENDIX

Defined parameters

$$k_s = \frac{L_m}{L_s}, k_r = \frac{L_m}{L_r}, L_s{}' = L_s - \frac{L_m{}^2}{L_r}, L_r{}' = L_r - \frac{L_m{}^2}{L_s}$$

$$A1 = \frac{dab}{b^2+c^2} - e \ , \ B1 = \frac{acd}{b^2+c^2} + f \ , \ C1 = -p\varphi_{rq0},$$

$$D1 = \left[\left(\frac{d}{b^2+c^2}\right)\left(b\varphi_{sq0} - c\varphi_{sd0}\right) + \varphi_{rq0}\right]$$

$$A2 = \frac{ab^2d}{c(b^2+c^2)} - \frac{ad}{c} - f \ , \ B2 = \frac{abd}{b^2+c^2} - e \ , \ C2 = p\varphi_{rd0},$$

$$D2 = \left(\frac{db}{c(b^2+c^2)}\right)\left(b\varphi_{sq0} - c\varphi_{sd0}\right) - \frac{d\varphi_{sq0}}{c} - \varphi_{rd0}$$

$$A3 = g\left(\begin{array}{l} -\frac{ab\varphi_{rq0}}{b^2+c^2} + \frac{ab^2\varphi_{rd0}}{c(b^2+c^2)} - \frac{a\varphi_{rd0}}{c} \\ +\varphi_{sq0} \end{array}\right)$$

$$B3 = g\left(-\frac{ac\varphi_{rq0}}{b^2+c^2} + \frac{ab\varphi_{rd0}}{b^2+c^2} - \varphi_{sd0}\right)$$

$$C3 = 0,$$

$$D3 = g\left(\begin{array}{l} \frac{-\varphi_{rq0}\left(b\varphi_{sq0} - c\varphi_{sd0}\right)}{b^2+c^2} \\ +\frac{\varphi_{rd0}\left(b^2\varphi_{sq0} - bc\varphi_{sd0}\right)}{c(b^2+c^2)} - \frac{\varphi_{rd0}\varphi_{sq0}}{c} \end{array}\right)$$

$$a = \frac{K_r R_s}{L_s{}'} \ , \ b = \frac{R_s}{L_s{}'} \ , \ c = \omega_{s0} \ , \ d = \frac{K_s R_r}{L_r{}'} \ , \ e = \frac{R_r}{L_r{}'}$$

$$, f = \omega_{s0} - p\Omega_{m0} \ , \ g = \frac{pK_r}{L_s{}'}$$

$$S1 = \frac{(B2*C2 - C2*B1)}{(B1*A2 - A1*B2)} \ , \ S2 = \frac{(B2*D1 - D2*B1)}{(B1*A2 - A1*B2)}$$

$$S3 = -\frac{A1*S3}{B1} - \frac{C1}{B1} \ , \ S4 = -\frac{A1*S2}{B1} - \frac{D1}{B1}$$